PTI Journal *Technical Paper*

NONLINEAR FINITE ELEMENT ANALYSES OF UNBONDED POST-TENSIONED SLAB-COLUMN CONNECTIONS

By

THOMAS H.-K. KANG AND YU HUANG

Authorized reprint from: July 2012 issue of the PTI Journal

NONLINEAR FINITE ELEMENT ANALYSES OF UNBONDED POST-TENSIONED SLAB-COLUMN CONNECTIONS

by Thomas H.-K. Kang and Yu Huang

The principal aim of the study is to develop a nonlinear finite element model for unbonded post-tensioned (PT) concrete slab-column connections using existent modeling techniques, along with an innovative technique that involves a combination of spring elements and an embedding technique to simulate the interaction between unbonded tendons and concrete. Two reinforced concrete (RC) slab specimens and four unbonded post-tensioned slab specimens tested by other researchers were introduced to verify the proposed numerical model. Nonlinear analyses showed that the damaged plasticity concrete constitutive model with proper parameters agreed well with experimental results. The nonlinear model of unbonded PT slabs adequately simulated the unbonded tendon slips as well as the overall responses of PT slab-column connections that failed in flexure followed by punching. The unbonded tendon modeling method was thus demonstrated to be a feasible way to simulate unbonded PT system behavior. Additionally, ACI 318-08 punching shear provisions were evaluated using the developed nonlinear finite element models of four PT connections, particularly for the fraction factor of γ_v *used in the eccentric shear stress model and the punching shear stress capacity* v_c *of PT connections.*

KEYWORDS

Finite element modeling; post-tensioned concrete; punching shear failure; reinforced concrete; slab-column connections; unbonded tendons.

INTRODUCTION

Even though finite element modeling techniques are becoming highly sophisticated, a steel reinforced concrete (RC) simulation is still troublesome when concrete is subject to three-dimensional (3-D) stress conditions, and a concrete slab-column connection is always in such a complex stress state (Kang et al. 2009). Due to the lack of robust concrete models in finite element programs, concrete analysis frequently suffers numerical difficulties such as convergence and accuracy problems. Furthermore, modeling unbonded post-tensioning (PT) tendon behavior is more difficult when dealing with the interaction between unbonded tendons and concrete. Available tube-to-tube contact techniques can achieve the goal of simulating the physical behavior of unbonded post-tensioned systems (refer to Huang et al. 2010); however, these techniques are impractical due to their high numerical cost. As such, PT concrete modeling is also one of the toughest topics for finite element researchers.

The nonlinear behavior of concrete slab-column connections, particularly for PT connections, has hardly been studied using the nonlinear finite element method. To address this gap, a series of nonlinear finite element analyses was performed on the concrete slab-column connections with and without the presence of unbonded PT reinforcement. In this study, a built-in damaged plasticity concrete model in ABAQUS (Abaqus 2003) was employed, and spring elements were introduced to simulate the interaction between unbonded PT tendons and concrete. For verification of the damaged plasticity concrete model, two lightly reinforced concrete slab-column connections tested by other investigators (Tian et al. 2008) were modeled. The lightly reinforced concrete slabs are selected to make relevant comparisons with PT slabs, which were also lightly reinforced with PT tendons. Subsequently, test results of four PT slab-column connections (Foutch et al. 1990) were used to calibrate the proposed model for unbonded PT tendons. Finally, investigations were made to evaluate the performance of exterior PT slab-column connections under monotoni-

PTI JOURNAL, V. 8, No. 1, July 2012. Received and reviewed under Institute journal publication policies. Pertinent discussion will be published in the next issue of *PTI JOURNAL* if received within 3 months of the publication.

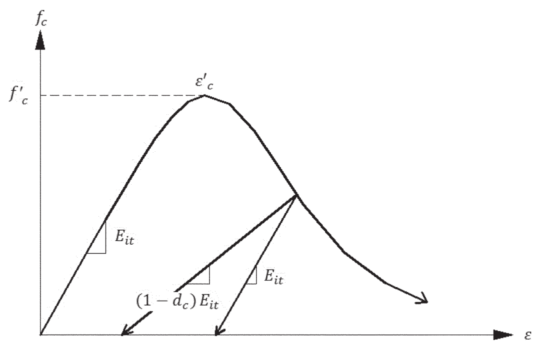

Fig. 1—Damaged plasticity model for concrete in compression used in experiment.

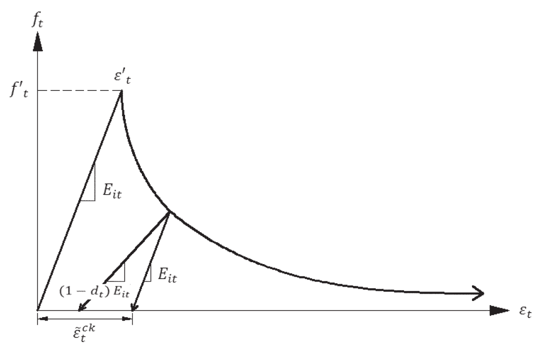

Fig. 2—Used concrete tension model accounting for tension stiffening effects.

cally increasing unbalanced moments by integrating the innovative numerical simulation technique.

MATERIAL AND ELEMENT MODELING

In this section, modeling approaches are summarized, including the unbonded tendon and tendon anchorage models. Also, this section summarizes models presently used for materials (concrete and steel), elements, and meshing. The theoretical background to this work and more details of the procedure used in multi-scale modeling of unbonded post-tensioned concrete structures are provided by Huang et al. (2010).

Concrete modeling

A built-in damaged plasticity model in ABAQUS (Abaqus 2003) was employed for concrete modeling in the numerical analysis. The damaged plasticity model provides a general capability to model concrete and other quasi-brittle materials in all types of structures (for example, beams, trusses, shells, and solids). This model is based on the assumption that concrete fails either due to tension cracking or compressive crushing. In this analysis, no considerations were given to concrete damage during unloading (that is, the damage factors [d_c and d_t] are set to zero; refer to Fig. 1 and 2), as it has been confirmed that the results under monotonic loads were not sensitive to the tension damage factors. This is because there was no cyclic loading involved. The neglect of the compression damage factors would also be reasonable because the slab tends to be governed by tension cracking failure, as noted in another section.

Compression behavior

The damaged plasticity model requires a uniaxial stress-strain relationship definition for plain concrete in compression. An empirical stress-strain relationship model (Carreira and Chu 1985) was used to define the monotonic stress-strain relationship (Fig. 1). This model is expressed as follows

$$\frac{f_c}{f_c'} = \frac{1000\beta(\varepsilon/\varepsilon_c')}{\beta - 1 + (\varepsilon/\varepsilon_c')^{\beta}} \tag{1}$$

$$\beta = \frac{1}{1 - [f_c'/(\varepsilon_c E_{it})]} \tag{2}$$

$$\varepsilon_c' = (0.00488 f_c' + 168) \times 10^{-5} \tag{3}$$

where f_c is the concrete compressive stress (variable); f_c' is the concrete compressive strength in psi; ε is the concrete compressive strain (variable); ε_c' is the concrete strain corresponding to f_c'; and E_{it} is the initial tangent modulus of elasticity, in psi. The measured properties of f_c' were used in the numerical analysis (Table 1). The original research by Carreira and Chu (1985) suggested obtaining E_{it}, either from a standard elastic modulus test or an equation in the ACI 318 Code. In this study, because the ACI 318 equation overestimates E_{it} for high-strength concrete, the following equation was adopted as recommended by Nilson et al. (2009)

$$E_{it} = 40{,}000\sqrt{f_c'} + 1{,}000{,}000\left(\frac{w_c}{145}\right)^{1.5} \tag{4}$$

where w_c is the unit weight (= 145 lb/ft^3 in this study) of the concrete, in lb/ft^3. The stress-strain curve calculated using Eq. (1) to (4) was simplified to a multi-linear fit as input into the ABAQUS program (Abaqus 2003), as shown in Fig. 1.

Tension behavior

The tension stiffening effect was considered in the concrete-damaged plasticity model. The tension stiffening effect can be modeled by either using a stress-strain rela-

Table 1—Material and post-tensioning properties used for modeled specimens

Specimens		f_c', ksi	f_t', psi	$\tilde{\varepsilon}_t^{ck}$	f_{res}, psi	f_y, ksi		E_s, ksi	f_{pc}, psi		f_{pe}, ksi	
						No. 3	No. 4		W-E	N-S	W-E	N-S
RC0.5	Tension Model 1	4.55	500	1×10^{-10}	30	59	61	29,000	NA	NA	NA	NA
	Tension Model 2			0.000287								
	Tension Model 3			0.00014								
RC1.0	Tension Model 1	4	475	1×10^{-10}	47	59	61	29,000	NA	NA	NA	NA
	Tension Model 2			0.000287								
	Tension Model 3			0.00014								
S1	Tension Model 1	7.3	726	1×10^{-10}	70	73	NA	28,300*	650	246	166.8	138.9
	Tension Model 2			0.000316								
	Tension Model 3			0.00015								
S2		6.2	627	0.00029	30	73	NA	28,300*	691	325	177.4	183.5
S3		6.1	702	0.000337	70	73	NA	28,300*	260	385	183.5	181.2
S4		7	628	0.000286	60	73	NA	28,300*	264	368	186.4	173.2

*Modulus of elasticity for tendons.
Note: W-E is tendons placed perpendicular to slab edge; N-S is tendons placed parallel to slab edge; and NA is not available.

tionship or setting a fracture energy cracking criterion (Hillerborg et al. 1976). The stress-strain relationship input method was used herein, as the fracture energy cracking criterion requires solid elements with a relatively small aspect ratio, which is inconvenient for modeling PT systems (for example, end anchorage, unbonded tendons).

The tension stiffening effect simulates the interaction between concrete and deformed bars when cracking occurs. It is assumed that the residual stress f_{res} in concrete after cracking is a function of cracking strain $\tilde{\varepsilon}_t^{ck}$ (refer to Fig. 2). For heavily reinforced members, tension stiffening is suggested such that the stress reduces to zero at a total strain of approximately $10\varepsilon_t'$ (Abaqus 2003), where ε_t' is the strain corresponding to the tensile strength f_t'. For RC slabs, however, such a large tension stiffening effect would introduce unreasonable mesh sensitivity because no reinforcement is provided in some cracked regions. Therefore, the tension stiffening effect is carefully considered as described in the following paragraph.

The first approach was to set the cracking strain $\tilde{\varepsilon}_t^{ck}$ to a sufficiently small value (10^{-10}) without tension stiffening in ABAQUS (Abaqus 2003) (Tension Model 1; refer to Fig. 3); however, this model may not represent the actual tension behavior of concrete. An alternative solution was to increase tension stiffening (for example, gradually descending slope after f_t' [Tension Model 2; refer to Fig. 3]) by assuming the cracking strain $\tilde{\varepsilon}_t^{ck}$ as equal to approximately twice the strain corresponding to ε_t' (strain corresponding to f_t') (Table 1). This model saves computational cost, as it would increase the minimum stable time increment in explicit analysis. The third approach was to model such that when cracking occurs, the stress will suddenly drop to a small value (f_{res}) required to just maintain calculation stability (that is, small tension stiffening) (Tension Model 3; refer to Fig. 3). The values of f_{res} used in the analysis are provided in Table 1. This model also tends to cause numerical difficulties because of the sudden drop in stress, which leads to dramatic stress redistribution within a very short time that results in a very slow convergence rate and a local cracking failure. These three models for concrete in tension are compared, and their accuracy and feasibility are discussed in another section. The experimental data of the modulus of rupture, where available, or the values calculated using the ACI 318 equation for f_r ($= 7.5\sqrt{f_c'}$) are used to define the values of f_t' (Table 1).

Bonded mild steel modeling

A bilinear stress-strain relationship (along with f_y and E_s) is reasonably accurate to define the behavior of nonprestressed bonded bars. The values of f_y and E_s used to define the bilinear relationships are indicated in Table 1.

The interaction between deformed reinforcing steel and concrete is considered as a perfectly bonded condition. Perfect bonding can be achieved by using an embedding technique in ABAQUS (Abaqus 2003), in which the

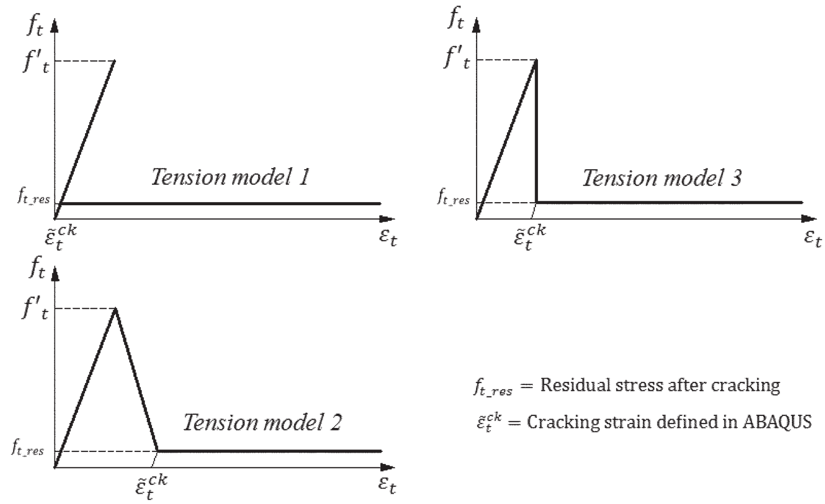

Fig. 3—Three different tension stiffening models used in experiment.

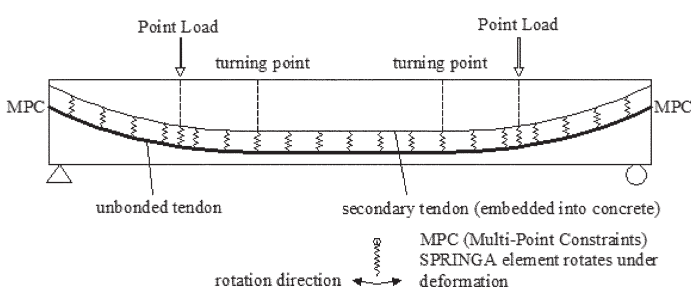

Fig. 4—Unbonded PT tendon modeling.

displacement of steel bars is compatible with that of the concrete element. Note that the objective of the study is not to assess the ultimate failure, but to observe the stress distribution and redistribution during the loading when bond-slip is not a serious concern. Also, bonded steel in PT slabs tends not to slip. This is evidenced by the fact that, in this study, analytical results correlate well with experimental data (except at ultimate failure), with the assumption of perfect bonding.

Unbonded PT tendon modeling

The empirical stress-strain model developed by Devalapura and Tadros (1992) was adopted as a model for Grade 270 seven-wire strands. This model is shown in the following power formula

$$f_{ps} = \varepsilon_{ps}\left[A + \frac{B}{(1+(C\varepsilon_{ps})^D)^{1/D}}\right] \le f_{pu} \tag{5}$$

where f_{ps} is the stress in the strand (variable), in ksi; ε_{ps} is the strain in the strand (variable); and A, B, C, and D are the power constants of 887, 27, 623, 112.4, and 7.37, respectively, determined based on the lower bound of 56 tendon test curves by Devalapura and Tadros (1992). The tendon stress-strain curve was then simplified to a multilinear fit for ABAQUS input (Abaqus 2003).

The nature of unbonded tendon behavior introduces a highly nonlinear boundary condition that is usually referred to as the so-called contact problem. The feasibility of simulating unbonded tendon behavior using the available contact modeling capabilities is highly questionable due to the significant modeling efforts and computational cost (Huang et al. 2010). Therefore, an alternative way to simulate unbonded tendon behavior in the traditional nonlinear analysis is desired. The boundary nonlinearity can be eliminated by using the axial spring system method, as explained in the following paragraph.

The tendon can slip along the tube in concrete under deformation. The unbonded interaction can be modeled using the SPRINGA element of ABAQUS (Abaqus 2003). This element is composed of the rigid link between two nodes, which can free-rotate around the nodes under large member deformations (Fig. 4). For the unbonded tendon modeling, almost infinite spring stiffness (that is, rigid axial spring) was adopted to allow the constant distance between two nodes that simulates tendon slip motions. A relatively large number of spring elements (that is, two to three springs per foot) was used for an internal unbonded system to obtain adequate accuracy; however, a sensitivity study conducted by Huang et al. (2010) revealed that the quantity of spring elements hardly influenced the final results if the springs were located in necessary locations (for example, at points of inflections or the location on which the point load acts) with a reasonable density. More details on the tendon modeling approaches are provided by Huang et al. (2010).

To avoid the concrete stress concentration that may result if the spring element is directly attached to the concrete node, an additional virtual tendon element can be embedded in the concrete element with a distance of approximately one-quarter of the slab thickness from the real tendon (Fig. 4). The distance between virtual and actual tendons does not affect the result (Huang et al. 2010). As such, this additional tendon element is connected between the spring element and the concrete element. The secondary tendon element is taken to have a negligible stiffness. The balancing vertical loads generated by post-tensioning forces are transferred from the real tendon to the concrete. Additional restraints are placed to eliminate the tendon motion in the transverse direction to the direction of the tendon.

In the experimental program that is used for the calibration with numerical modeling (Foutch et al. 1990), the friction was found to be insignificant due to a relatively short distance between the anchorages. Even for a long distance between the anchorages, once a certain amount of loading is applied (after substantial tendon movement with respect to the concrete), essentially no friction exists between the tendons and the concrete because of the bond breaking. This has been experimentally verified by Kang and Wallace (2008).

End anchorage modeling

The so-called multi-point constraints (MPCs) were imposed to constrain nodes with different coordinates. ABAQUS (Abaqus 2003) provides a variety of MPC functions. In this analysis, the Beam MPC was used to simulate the tendon end anchorage. The Beam MPC provides a rigid beam between nodes, which can be used to simulate the compatibility of deformations between the unbonded tendon and anchorage.

ABAQUS/Standard versus ABAQUS/Explicit

Although ABAQUS/Standard (Abaqus 2003) is suitable for a nonlinear static problem, numerical convergence problems often occur because of highly nonlinear material failures such as cracking behavior with small tension stiffening. Only Tension Model 1 without tension stiffening works properly with the implicit analysis. When a loading rate is sufficiently small (that is, quasi-static), a dynamic explicit analysis also functions well without any convergence difficulty. The dynamic explicit analysis consumes more computational cost, but offers more freedom to adjust the model (for example, adjustments of tension stiffening). Therefore, the dynamic explicit analysis provided by ABAQUS/Explicit (Abaqus 2003) is preferred in the numerical study. The results based on the implicit (along with Tension Model 1) and explicit (along with Tension Model 2 and Tension Model 3) analyses are compared in another section.

The PT force was simulated by applying a predefined tendon stress state in ABAQUS/Standard (Abaqus 2003). The exact value was obtained after the iteration of preliminary analysis until the effective prestress f_{pe} in the tendon was at the desired level. On the other hand, the PT force was given by using a "temperature field via cooling tendons" in ABAQUS/Explicit (Abaqus 2003). Also, several iterations were done to obtain the desired effective prestress f_{pe}.

Dilation angle and viscosity parameter

A fixed dilation angle of 50 degrees was calibrated and used for all of the specimens modeled in this study. In general, a smaller dilation angle, such as 30 to 40 degrees, is defined in the damaged plasticity model; however, when the concrete is subject to a 3-D stress state (for example, slab or other element under confinement), a larger value would be appropriate to simulate the actual behavior of the concrete (Abaqus 2003). From preliminary simulations, a slight difference in overall nonlinear response has been observed with different dilation angles except the failure point (for example, instant at which failure initiates). Also, shear stress histories around the critical section were almost the same for models with different dilation angles. It is noted that accurate detection of punching failure was not the focus of the study, rather, it was to give an accurate picture of 3-D stress states both before and after stress redistribution at the connection. Therefore, a constant dilation angle of 50 degrees was used.

In terms of the viscosity parameter, a very small value of 0.0005 (one order of magnitude less than the typical time increment) was adopted for implicit analysis to produce an improved convergence rate. The default value of zero for the viscosity parameter was used because it was not a concern for the explicit analysis. All other parameters needed for the damaged plasticity model were set to default values as specified in ABAQUS (Abaqus 2003).

Elements

The ABAQUS element library (Abaqus 2003) includes abundant continuum elements in 3-D formulation. In this

Table 2—Representative results from both experiments and analyses for several displacement or shear force steps (for RC specimens)

	RC0.5		RC1.0	
Center displacement, in.	Gravity load, kips		Gravity load, kips	
	FEA	EXP	FEA	EXP
0.2	38.8	36.4	47.1	47.8
0.4	51.7	48.5	63.7	65.8
0.6	60.6	60.3	78.1	80.1
0.8	64.5	66.6	84.1	86.3

	RC0.5						RC1.0					
V/V_{ult}	Strain ($\times 10^{-3}$)						Strain ($\times 10^{-3}$)					
	T-1		T-10		B-1		T-1		T-10		B-1	
	FEA	EXP	FEA	EXP	FEA	EXP	FEA	EXP	FEA	EXP	FEA	EXP
0.2	0.04	0.01	0.03	0.01	–0.05	–0.04	0.05	0.04	0.04	0.02	–0.07	–0.05
0.4	0.34	0.07	0.02	0.05	–0.12	–0.08	0.65	0.35	0.048	0.044	–0.22	–0.1
0.6	1.16	1.07	0.5	0.71	0.08	0.33	1.37	1.15	0.87	0.58	0.18	0.3
0.8	2.04	1.95	1.54	1.76	0.6	1.24	2.07	2.04	1.45	1.21	0.73	0.77

Note: FEA results from model using Tension Model 2.

analysis, the eight-node first-order element (C3D8R) with one reduced integration rule was used for both implicit and explicit analyses for three reasons: 1) the quadratic element is not available in the explicit element library; 2) the first-order reduced integration element greatly saves computational cost; and 3) the reduced integration element avoids shear locking that would be a problem in the first-order full integrated element.

Bonded reinforcing steel and PT tendons were modeled using two-node truss elements (T3D2) embedded within the concrete elements. The specimens were modeled using four (for RC slabs) or five (for PT slabs) layers of concrete elements (that is, four or five integration points lie along a vertical line) to properly model the stiffness of the slab. It is noted that 3-D RC slabs can also be simulated using a different finite element methodology that uses nine-node Lagrange Mindlin shell elements (for example, Park and Choi 2006); however, the selected elements are more applicable to a developed unbonded PT modeling method.

The RC and PT specimens have various mesh sizes of 2 to 6 in. (50.8 to 152.4 mm) depending on the location. The finer mesh size was used in the connection region due to a high degree of cracking. More details are available in Huang et al. (2010).

MODEL VERIFICATION

In the preceding section, a variety of adopted or developed modeling approaches were described, including modeling for concrete, steel (bonded and unbonded), and tendon end anchorage. This section provides verification of these approaches through modeling studies of previously tested specimens of RC and PT slab-column connections. Tables 2 and 3 summarize representative results from both experiments and analyses for several displacement, shear force, or moment steps. From the studies on the RC slabs, the capability of the modeling techniques for materials, elements, and meshes is verified, whereas the modeling studies on PT slabs verify the modeling techniques for the effects of unbonded tendons and end anchorages.

RC slab-column connections

Test specimens selected for nonlinear finite element modeling

Two RC interior slab-column connections (G1.0 and G0.5) tested by Tian et al. (2008) were selected as specimens for model verification (Fig. 5). Specimen G1.0 had more top reinforcing bars placed within the width of (c_2 + 3h) than G0.5. The top reinforcing ratios within c_2 + 3h were 1% and 0.5% for G1.0 and G0.5, respectively, and 0.4% outside (c_2 + 3h) for both G1.0 and G0.5. All bottom reinforcement was discontinued at the interface of two spans (that is, at the support line). The bottom reinforcing ratio was 0.1% for both G1.0 and G0.5. The slab thickness, square column size, and span-to-thickness ratio were 6 , 16, and 28 in. (152.4, 406.4, and 711.2 mm), respectively. The one-story column (half a story above and below the slab) was assumed to remain elastic due to the design of the strong column weak slab.

Table 3—Representative results from both experiments and analyses for several moment steps (for PT specimens)

S1			S2			S3			S4		
Moment, kip-ft	Stress increase, ksi		Moment, kip-ft	Stress increase, ksi		Moment, kip-ft	Stress increase, ksi		Moment, kip-ft	Stress increase, ksi	
	FEA	EXP		FEA	EXP		FEA	EXP		FEA	EXP
20	–0.25	0.25	20	–0.05	0.1	20	1.8	1	15	0	0.4
25	0.1	0.6	25	0.1	0.4	23	3	2.5	20	1.5	1.5
30	1.5	1.5	30	0.9	1.25	26	4.7	5	22	2.2	2.4
35	2.4	3.2	34	2	2.75	28	8	8	24	2.8	3.6
42	11.2	9.5	37	3.2	5.2	30	14.9	13.7	26	5	6

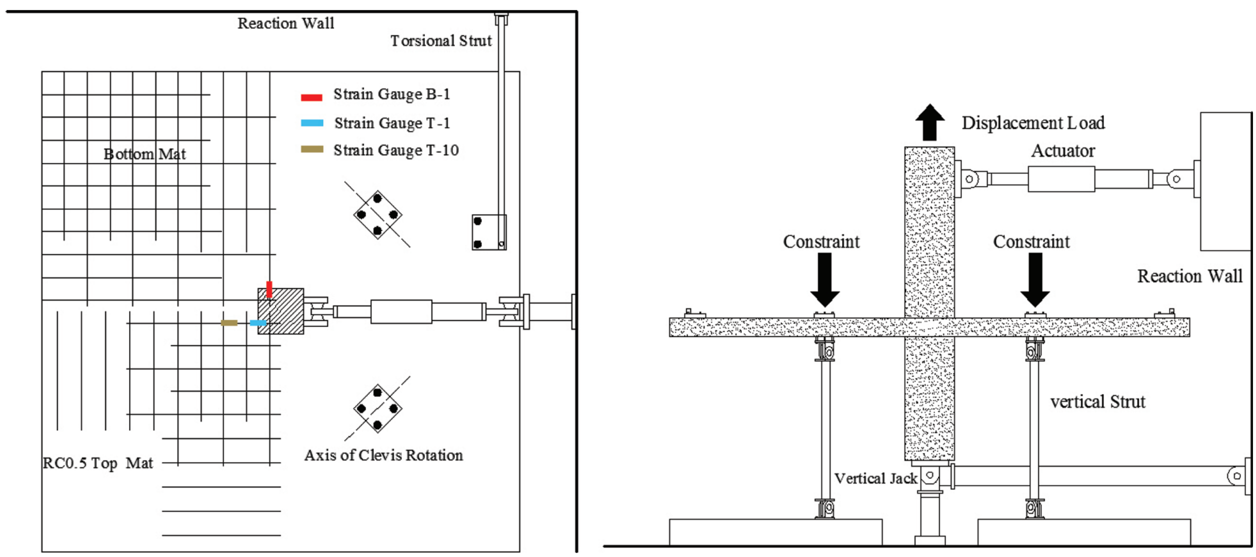

Fig. 5—Test configuration and strain gauge instrumentation for two interior RC slab-column connection specimens.

While the bottom of the column was monotonically loaded (lifted) to failure, four struts were used to restrain the slab displacement to simulate the increasing gravity loads on slabs. The column top was pinned to the wall. The measured concrete strength f_c' was 4060 and 4550 psi for G1.0 and G0.5, respectively. The measured steel yield stress f_y was 61 and 59 ksi for top and bottom reinforcement at the connection, respectively. Detailed information is provided by Tian et al. (2008).

Results from nonlinear finite element modeling

Given the symmetry in geometry, loading, and boundary conditions, one-quarter of the slab and column was modeled. First, analytical responses of Specimens G1.0 and G0.5 using three different tension stiffening models are compared, along with experimental data. Figure 6 shows that all three of the models captured the actual nonlinear behavior of the RC slab-column connections quite accurately, except for failure detection. Only negligible effects of changes in tension stiffening on the nonlinear behavior were found, because the changes in tension stiffening across the three different models were relatively small. Similar results are expected for PT slabs, and this is verified in the following section. For more detailed analyses of the RC connections, Tension Model 2 (refer to Fig. 3) was selected due to its numerical stability.

Figure 7 shows comparisons between experimental and analytical results of steel strains obtained with Tension Model 2 for tension stiffening. The finite element analysis reproduced the strain in the bonded reinforcement reasonably well. The discrepancy at the end of the response might be due to the bond slip that was observed just before or at failure during the experiment. The bond-slip effect was not modeled in this study. In conclusion, the analytical approaches developed in this study correlated quite well with both the global and local nonlinear responses of RC slab-column connections up to punching failure. This demonstrates the feasibility of the following modeling elements: 1) the bonded steel model (as well as

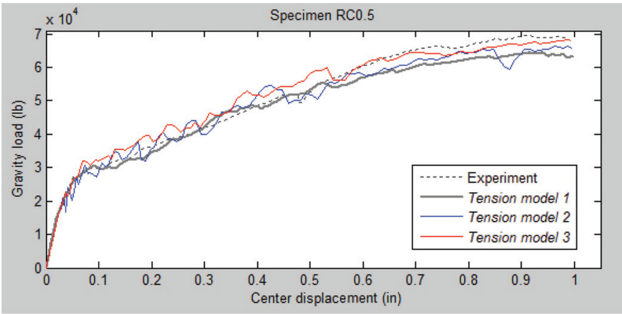

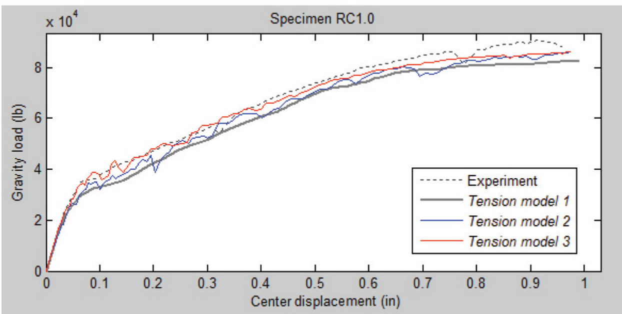

Fig. 6—Modeling of RC slab-column connections (RC0.5 and RC1.0).

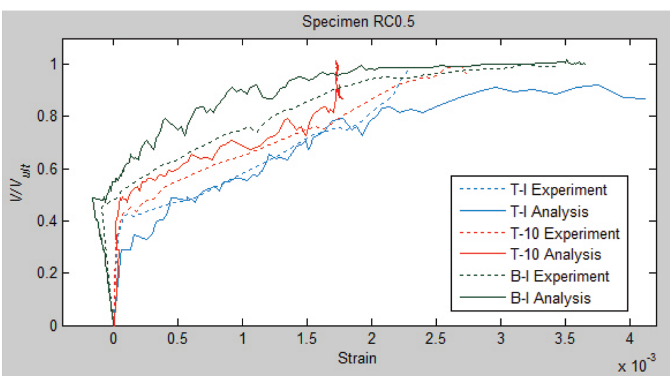

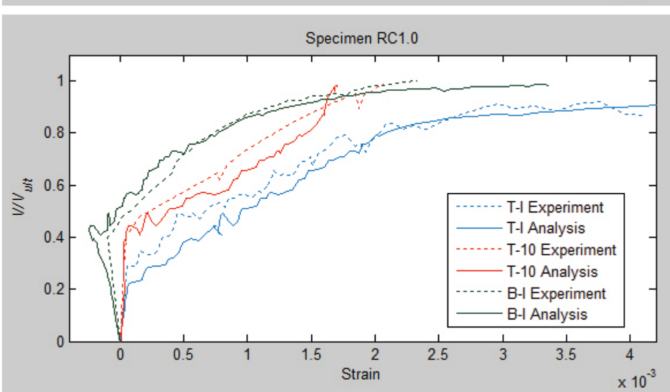

Fig. 7—Reinforcing bar strains monitored from experiments and analyses of RC slabs (V: applied shear; V_{ult}: measured ultimate shear; T: top bars; B: bottom bars; I: at the slab-column interface; 10: at 10 mm from the slab-column interface; refer to Fig. 5 for the location).

interaction between the steel and concrete); 2) concrete models for compression and tension; 3) the dynamic explicit analysis with Tension Model 2; and 4) the selection of elements, meshes, dilation angle, and viscosity parameter.

PT slab-column connections

Test specimens selected for nonlinear finite element modeling

Four PT slab-edge column connections tested by Foutch et al. (1990) were selected to evaluate the developed unbonded PT modeling method. Test specimen dimensions and reinforcing details are depicted in Fig. 8. The half-story column above and below the slab was pinned at each end. In the first two specimens (S1 and S2), tendons were banded perpendicular to the exterior edge of the slab. In the other two specimens (S3 and S4), tendons were banded parallel to the exterior edge of the slab, as presented by Fig 8. The No. 3 bars were used as crack-control steel reinforcement (top mild steel) in the vicinity of the column, and were also placed as top and bottom edge reinforcement around the perimeter of the slab to prevent splitting due to PT anchorage bursting forces (refer to the dashed lines in Fig. 8).

The only discrepancy between S1 and S2 or between S3 and S4 is the loading position (Fig. 8 and 9), which varies the moment-to-shear ratio. For each specimen, four equally distributed loading plates were placed parallel to the exterior edge of the slab, with the column pinned at both ends (top and bottom). Table 1 summarizes material properties and initial prestress (f_{pc} in concrete and f_{pe} in tendons) for test specimens. All PT tendons used were Grade 270 3/8 in. diameter, seven-wire strands. The average modulus of elasticity was 28,300 ksi. The tendons were inserted into 1/2 in. (12.7 mm) diameter polyethylene tubing to prevent bonding to the concrete. All bonded bars were Grade 60 steel with a measured yield stress of 72.7 ksi and an ultimate stress of 126.7 ksi. Detailed information is provided by Foutch et al. (1990).

Results from nonlinear finite element modeling

For the exterior connection, one-half of the slab and column was modeled due to its symmetry with respect to the axis perpendicular to the slab edge. The tendon located in the symmetry line was reduced to half the cross section of the original dimension for modeling symmetrical boundary conditions. For each specimen, approximately 75 to 100 spring elements were used to simulate the unbonded tendon behavior. Figure 9 illustrates finite element meshes and unbonded tendon modeling systems

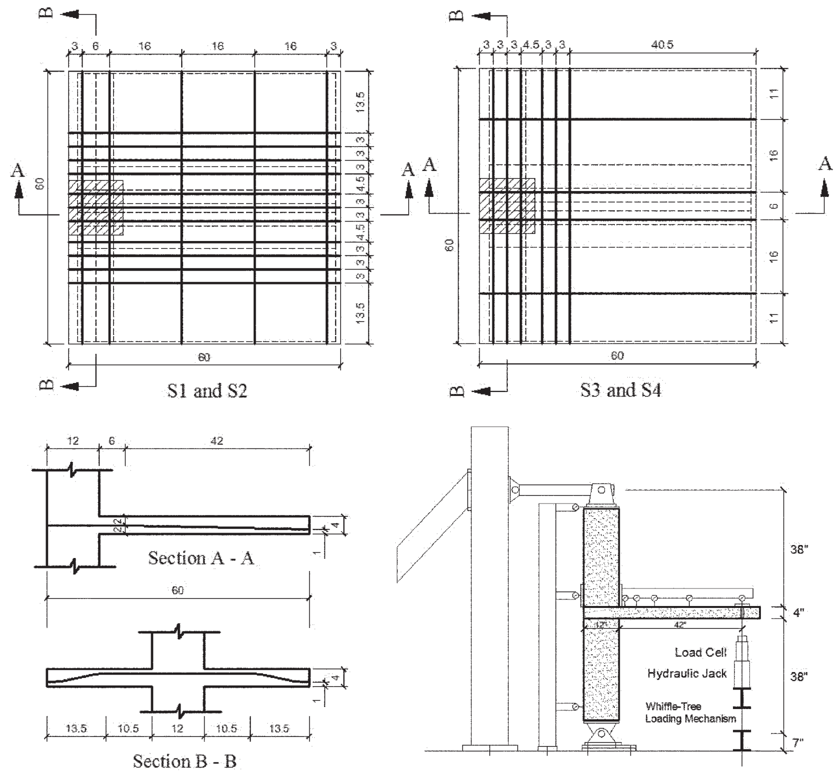

Fig. 8—Details and dimension of four edge PT slab-column connection specimens.

used for Specimens S3 and S4 (actual tendons in black and virtual tendons in blue). Every dot, except for tendon end anchorages, represents the location of a spring element.

Analytical responses of the PT connections modeled using three different tension models are compared, as they were for the RC connections (refer to Fig. 10 for Specimen S1 results). It is demonstrated that all three tension stiffening models exhibited comparable initial and ultimate behavior of the PT slabs. Particularly, the analyses using Tension Model 2 and Tension Model 3 yielded almost the same moment-drift relations at ultimate, indicating that the increase of tension stiffening did not substantially affect the ultimate capacity. Herein, the moment is defined as the total moment at the column face including both the applied load and the self-weight of the test specimen and setup, and the drift ratio is defined as the edge deflection divided by the distance between the column center and the point where the edge deflection is measured. For the detailed analysis (which was the rest of the analysis), Tension Model 2 was chosen.

Figure 11 depicts the comparison of the simulated and measured moment-versus-drift relations for Specimens S1 and S3 that failed in a flexural manner. The analytical results for Specimens S1 and S3 showed a fairly good agreement with

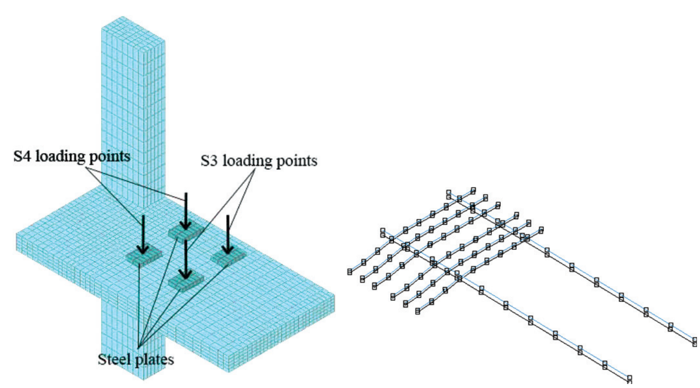

Fig. 9—Concrete finite element meshes and unbonded tendon modeling systems (half of one PT specimen; symmetric to the centerline of column).

the experimental results. Figure 12 compares the analytical and experimental results for Specimens S2 and S4 that failed in flexure followed by punching. Both Specimens S2 and S4 agreed reasonably well with the experimental data prior to punching shear failure. Although a slightly higher strength resulted than that found from the measured moment-drift relationships, general trends correlated fairly well with the test data. Furthermore, the PT connection damage patterns observed by Foutch et al. (1990) corre-

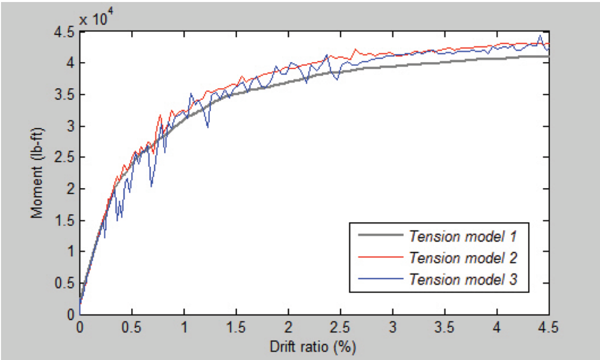

Fig. 10—Comparisons between three tension stiffening models used for PT slabs.

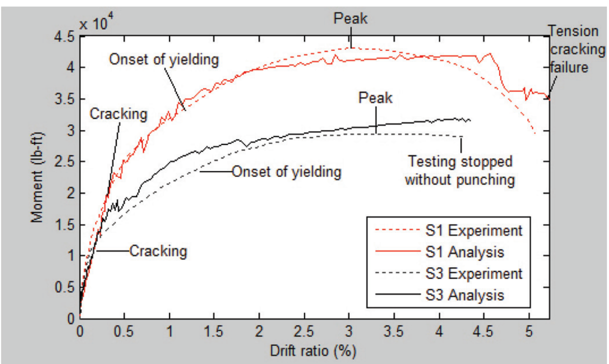

Fig. 11—Comparisons between experimental and analytical results for Specimens S1 and S3.

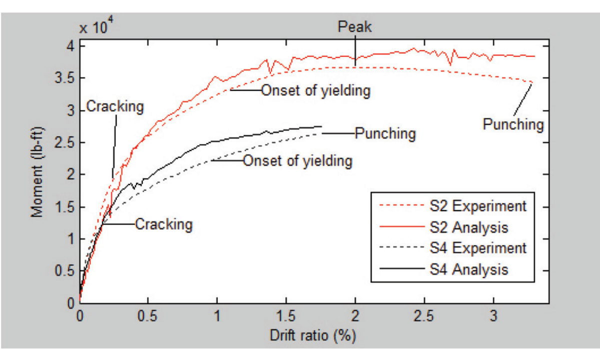

Fig. 12—Comparisons between experimental and analytical results for Specimens S2 and S4.

spond to the analytically predicted behavior (Huang et al. 2010). According to the deformations resulting from the analysis, Specimens S1 and S3 were simulated to experience very large slab rotations at the column face, whereas Specimens S2 and S4 were simulated to produce significant shear deformations near the column face. These are consistent with the test observations.

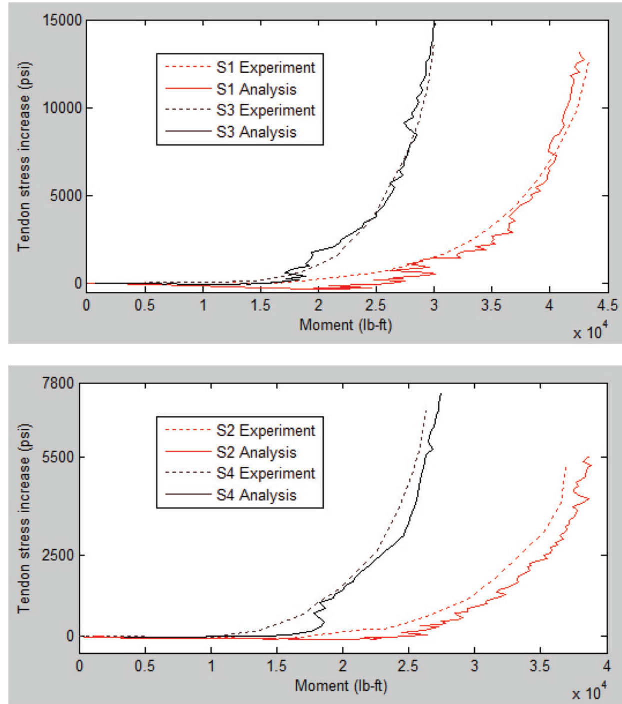

Fig. 13—Unbonded tendon stress increases versus applied moment.

Tendon stress values at multiple locations in a tendon were evaluated from the numerical model. The uniform tendon stress throughout the entire length was monitored from the analysis, which demonstrates that the unbonded tendon elongation was properly simulated. Figure 13 plots the maximum tendon stress development with increasing moment for the specimens. The tendon stress increases were in very good agreement with experimentally monitored increases, verifying that techniques for unbonded tendon modeling and end anchorage modeling are robust and accurate.

In this section, the accuracy of slab-column connection modeling approaches, including the innovative unbonded tendon model, has been demonstrated through modeling and calibrations of the global and local responses. In the following section, monitoring of shear stresses at desired locations at the shear critical section is attempted to investigate the fraction of unbalanced moment transferred by eccentric shear (γ_v). The following section also addresses the issue of the punching shear strength or stress capacity associated with PT edge slab-column connections.

ANALYSIS BASED ON THE ECCENTRIC SHEAR STRESS MODEL

Assessment of γ_v factor

Moment and shear transfers at slab-column connections are described in ACI 318-08, Section 11.11 (ACI

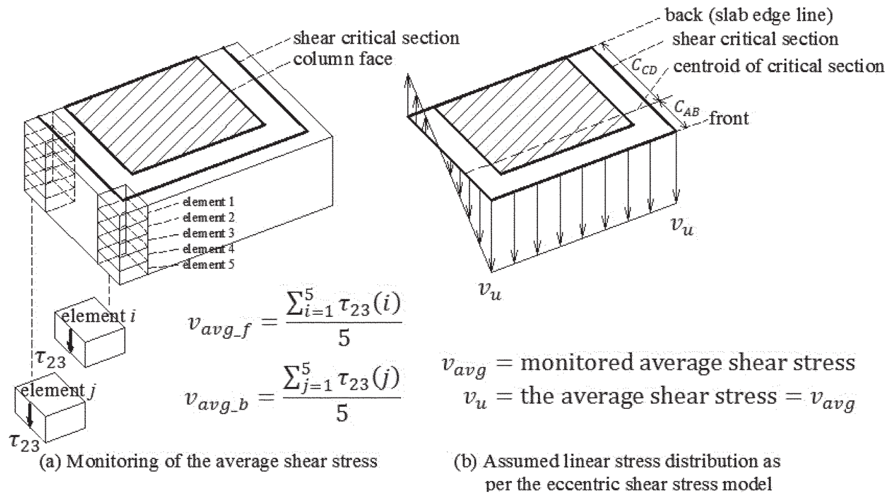

Fig. 14—Monitoring of direct and eccentric (torsional) shear stresses associated with eccentric shear stress model.

Committee 318 2008). ACI 318 code provisions present an empirical model—the so-called eccentric shear stress model—for designing shear and moment transfer on a critical section located at $(d/2)$ from the column face. The sum of direct shear and eccentric shear due to a fraction of unbalanced moment transfer may cause punching shear failure. A fraction of unbalanced moment given by $\gamma_f M_u$ is considered to be transferred by flexure, which suggests that the rest of the unbalanced moment, $\gamma_v M_u$, is assumed to be transferred by eccentric shear stress on the critical section. The fraction factors of γ_f and γ_v are given by ACI 318-08, Sections 13.5.3.2 and 11.11.7.1, respectively, as

$$\gamma_f = \frac{1}{1 + (2/3)\sqrt{(b_1/b_2)}} \tag{6}$$

$$\gamma_v = (1 - \gamma_f) \tag{7}$$

where b_1 is the width of the critical section measured perpendicular to the axis about which the moment acts, and b_2 is the width of the critical section transverse to b_1. For RC slab-column connections, ACI 318 allows the fraction of the unbalanced moment being transferred in flexure to be increased for both exterior and interior connections with relatively small gravity shear. The fraction factor of γ_f may be increased up to 1.0 for edge connections and $1.25\gamma_f$ for interior connections, if the factored gravity shear ratio $(V_u/\phi V_c)$ is not more than 0.75 and 0.4, respectively (Sections 13.5.3.3(a) and (b)), where V_u is the factored direct shear force to be transferred from the slab to the column, ϕ is the strength reduction factor of 0.75, and V_c is the nominal shear capacity provided by concrete. Also, to apply for the provision of Section 13.5.3.3(b), the net tensile strain ε_t at ultimate within the effective transfer slab width of an interior connection should not be less than 0.01. The Section 13.5.3.3 provision gives great flexibility in connection design; however, ACI 318-08 does not permit adjustments of γ_f or γ_v for prestressed (PT) connections. This calibration study aims to assess the validity of the model and provision, and to extend or improve the model, particularly the fraction factor of γ_v defined as part of the model.

Based on the well-developed finite element models, the value of γ_v has been evaluated for each PT specimen. The average shear stress along the slab thickness on a critical section has been monitored from integration points of the five layers (elements) located at the front or back corner of the shear critical section (refer to Fig. 14(a)). The analysis found that the shear stress on the side face at the front or back corner of the critical section was always the largest. The previous finite element analysis for RC exterior slab-column connections (for example, Park and Choi 2007) also reported similar results. The shear stress at this location, in accordance with ACI 318-08, is assumed to be equal to direct shear plus eccentric shear due to the fraction of unbalanced moment transfer (refer to Fig. 14(b)). The applied direct shear V_a and unbalanced moment V_{al}' were determined by statics, and the average shear stress v_u was directly obtained from the finite element analysis (Fig. 14(a)), where l' is the distance from the centroid of the critical section to loading point. The direct shear V_{sw} and unbalanced moment M_{sw} due to self-weight were collected at the location of the column center prior to

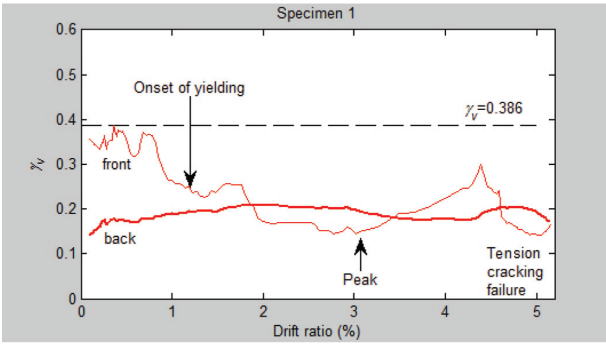

(a) S1

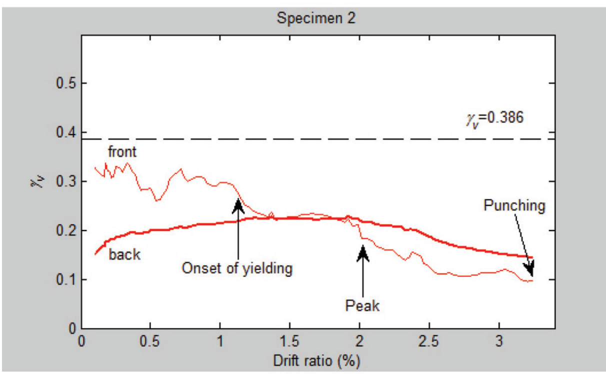

(b) S2

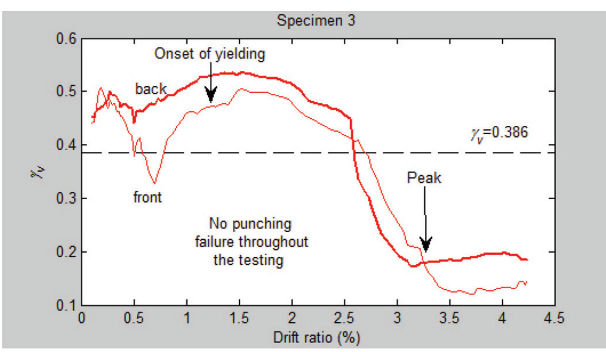

(c) S3

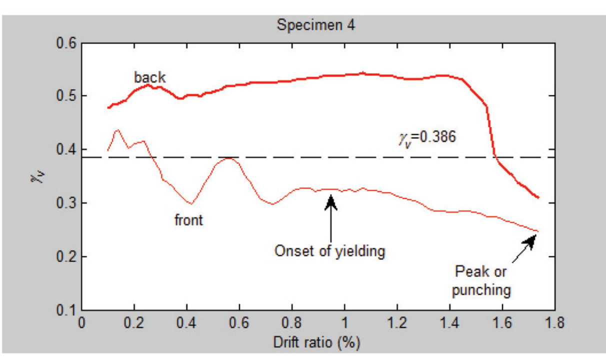

(d) S4

Fig. 15—Finite element results of fraction (γ_v) of unbalanced moment transferred by eccentric shear for edge PT slab-column connections.

the monotonic analysis. Finally, the value of γ_v was determined from the following equations

$$v_u = \frac{(V_{sw} + V_a)}{A_c} + \frac{\gamma_v (M_{sw} - V_{sw} g + V_a l')c_{AB}}{J_c} \tag{8}$$

$$v_u = \frac{(V_{sw} + V_a)}{A_c} - \frac{\gamma_v (M_{sw} - V_{sw} g + V_a l')c_{C'D'}}{J_c} \tag{9}$$

where A_c is the area of shear critical section specified in ACI 318-08; g is the distance from the centroid of the critical section to the column center; $c_{C'D'}$ = (c_{CD} minus one-half the element dimension perpendicular to the slab edge at shear critical section = c_{CD} – 1.5/2 in.) (note that v_u is monitored slightly inside the slab edge and refer to element j in Fig. 14(a)); c_{AB} and c_{CD} are the distances from the centroid of the critical section to the perimeter of the critical section on the front end and back end (slab edge), respectively (refer to Fig. 14(b)); and J_c is the polar moment of inertia of the critical section (refer to Park and Gamble 2000, Section 10.3.3).

Figure 15 illustrates values of γ_v monitored at each loading step. Because flexural yielding of the bonded steel occurred prior to (or without) punching failure, which is common in a typical PT design, γ_v values in the inelastic deformation range or at peak strength of these specimens are primarily of interest. Beyond yielding (after 1% drift ratio, according to Foutch et al. 1990), the γ_v factor generally decreased as the load increased (that is, interaction between moment and shear decreased). The values at peak and punching or tensile cracking failure were less than those specified in ACI 318-08 (refer to dashed lines in Fig. 15). For example, the monitored values were only approximately half the specified value at peak or punching. It is notable that the γ_v values obtained from the front and back sides of the critical section (that is, from Eq. (8) and (9)) are quite consistent, which indicates that the eccentric shear stress model is valid for PT edge slab-column connections and that there is a certain degree of interaction between moment and shear at the PT edge connection, unlike the case of RC edge connections. Only the γ_v values at the front and back sides of Specimen S4 are quite different from each other, due to the small applied moment-to-shear ratio (that is, small l'; refer to Fig. 8), which is unlikely to occur in real cases. For small unbalanced moment (V_{al}'), the results are very sensitive to the variation of V_a.

According to the finite element results, Specimens S3 and S4 had quite large fractions (γ_v) of the unbalanced moment transferred by eccentric shear at the corner of the connection before yielding, whereas at peak or punching, the γ_v values of Specimens S3 and S4 were substantially decreased. The higher γ_v at lower drifts was related to the tendon arrangement. The shear stress of τ_{23} (refer to Fig. 14 for notation) was relatively large before the redistribution of shear stress because of large initial prestress (normal stress) from banded tendons parallel to the slab edge, and it was verified that the vertical shear stress was proportional to the initial normal stress of the element at the location. After the stress redistribution, the simulated behavior was similar to Specimens S1 or S2. The tendons placed adjacent to the column produced higher shear stress on the side critical section of Specimen S3 than Specimen S1, but did not cause serious shear damage, possibly due to the confining effects. A similar behavior was obtained in Specimen S4, which failed in punching shear. Note that Specimen S4 resisted a maximum shear stress substantially higher than the concrete shear stress capacity (dotted lines in Fig. 16). More discussions on the shear stress capacity are presented in the following section.

Although it may not be possible to make clear recommendations given the limited calibration exercise, application of reduced γ_v (for example, by 50%) may be allowable for edge PT slab-column connections transferring moment normal to the slab edge. This exercise is highly intriguing, and there is significant potential in further assessment of more PT edge slab-column connections and PT connections with lower precompression in concrete, different aspect ratios, and/or various loading and boundary conditions.

Assessment of punching shear stress capacity v_c

ACI 318-08, Section 11.12.2.2, defines the punching shear strength of an interior PT slab-column connection as follows

$$v_c = (\beta_p \lambda \sqrt{f_c'} + 0.3 f_{pc}) b_o d + V_p \tag{10}$$

where β_p is the smaller of 3.5 and ($\alpha_s d/b_o$ + 1.5, with α_s = 40, 30, and 20 for interior, exterior, and corner connections, respectively), if f_c' is in psi, λ is the lightweight concrete modification factor (λ for PT slabs with normalweight concrete = 1), b_o is the perimeter of the assumed critical section, d is the effective depth, f_{pc} is the average compressive stress in concrete due to the effective PT force for the full specimen width, and V_p is the vertical component of all effective PT forces crossing the critical section. The V_p term is approximately neglected, as the tendon

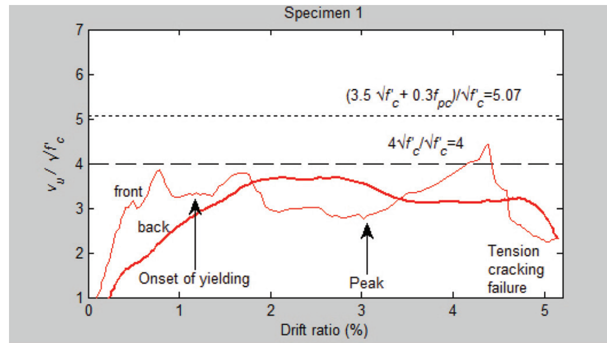

(a) S1

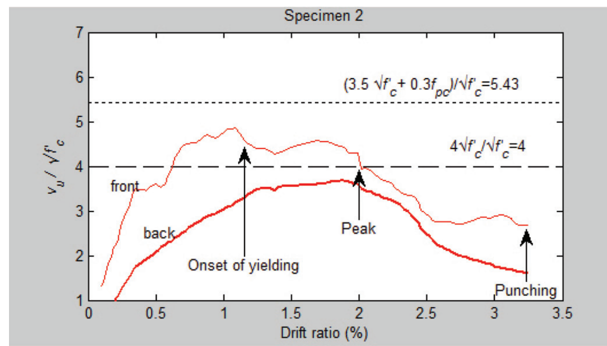

(b) S2

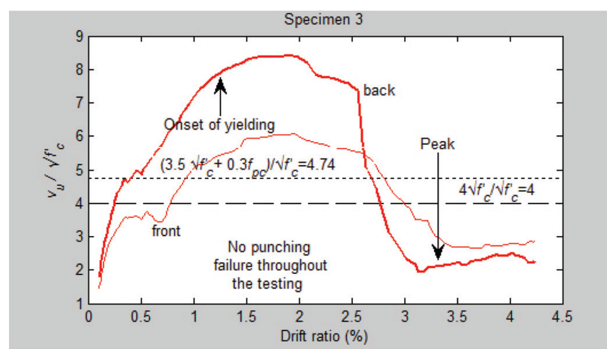

(c) S3

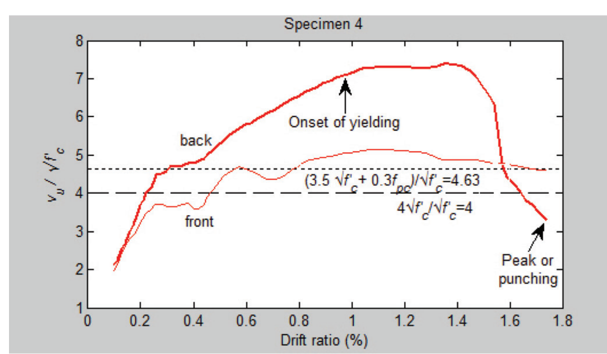

(d) S4

Fig. 16—Finite element results of average shear stress (v_u) at corner of critical section for edge PT slab-column connections.

Table 4—Shear stress demands and capacities calculated based on test data for PT specimens

Specimens	V_{sw}, kips	V_a, kips	M_{sw}, in.-kips	A_c, in.^{2}	l', in.	g, in.	c_{AB}, in.	c_{CD}, in.	J_c, in.^{4}	v_{u_AB}*, psi	v_{u_CD}*, psi	v_c†, psi	v_c‡, psi	v_{u_AB}§, psi	v_{u_CD}§, psi
1	2	3	4	5	6	7	8	8	9	10	11	12	13	14	15
S1	1.45	12.21	38.3	140.6	44.7	3.28	4.37	9.28	2242.7	533.5	–767.2	341.8	433.4	315.3	–335
S2	1.45	18.4	38.3	140.6	26.7	3.28	4.37	9.28	2242.7	533.5	–636.3	315	428	337.3	–247.6
S3	1.45	14.52	38.3	140.6	26.7	3.28	4.37	9.28	2242.7	427.6	–498.4	312.4	370.1	270.6	–192.4
S4	1.45	26.3	38.3	140.6	14.7	3.28	4.37	9.28	2242.7	508.6	–413.3	334.7	387.6	353	–107.9

*Shear stress calculated using values in this table and Eq. (8) or (9), with γ_v (= 0.386)
†Shear stress capacity calculated using values in Table 1 and ACI 318-08 (= $(4\sqrt{f'_c})$ psi)
‡Shear stress capacity calculated using values in Table 1 and Eq. (10) [= $3.5\,(\sqrt{f'_c} + 0.3f_{pc})$] psi
§Shear stress calculated using values in this table and Eq. (8) or (9), with γ_v (= 0.5 × 0.386)
Notes: Notation is same as used in Eq. (8) and (9), except the following: V_{sw} is experimentally measured direct shear due to self-weight of specimen and setup at centroid of critical section when V_a was reached (Foutch et al. 1990); V_a is peak applied load obtained from experiment (Foutch et al. 1990); and M_{sw} is experimentally measured unbalanced moment due to self-weight of specimen and setup at centroid of critical section when V_a was reached (Foutch et al. 1990).

profile was relatively straight with almost zero eccentricity for the scaled edge connection with a very small tributary slab area. Equation (10) is not permitted if the following limits of ACI 318-08 Sections 11.12.2.2(a), (b), and (c) are not satisfied:

(a) No portion of the column cross section shall be closer to a discontinuous edge than four times the slab thickness;

(b) The value of f'_c used in Eq. (8) and (9) (in this paper) shall not be taken greater than 70 psi; and

(c) In each direction, f_{pc} shall not be less than 125 psi, or be taken greater than 500 psi.

As indicated in Table 1, the PT specimens tested by Foutch et al. (1990) do not satisfy most of these limits. Primarily, according to Section 11.12.2.2(a), an edge PT slab-column connection is assumed to have smaller punching shear strength, which is equivalent to that of an RC slab-column connection without PT. ACI 318-08 Commentary R11.11.2.2 states that the prestress is not fully effective around the perimeter of the critical section near the slab edge. In this calibration study, investigation is focused on whether the aforementioned statement is the case and, if not, on how much concrete shear stress can be exerted on the critical section prior to punching failure, following flexural failure. Note that most typical PT connections experience flexural yielding followed by punching shear, and that the punching failure without yielding of bonded steel is quite a rare case of design.

Previous experimental research (Smith and Burns 1974; Trongtham and Hawkins 1977; Foutch et al. 1990) attempted to obtain the punching shear capacity of individual PT slab-column connections (without shear reinforcement) by monitoring applied shear and moment (measured). Actual stresses were not obtained from any of the previous tests, however, due to the difficulty in monitoring the applied shear force or stress at a point inside the concrete slab. Furthermore, there have been significant uncertainties of the effective transfer slab width, the fraction factor of γ_v, and the unbonded tendon stress at punching. Well-developed nonlinear finite element modeling, along with well-documented experimental data, innovatively solves this problem.

Figure 16 illustrates the variation of average shear stresses v_u at the front and back corner points of the critical section compared to the ACI 318-08 shear stress capacities of PT interior and exterior connections (v_c for exterior, shown using dots; and v_c for interior, shown using a dashed line). As depicted in Fig. 14(a), the average of the five layers' shear stresses was directly obtained from the finite element analysis at each loading step. Specimen S1 failed in a ductile manner with a very high moment-to-shear ratio (refer to Fig. 8). A flexural yield line was formed across the full width of the slab before the connection exhausted its capacity to transfer the unbalanced moment and shear. A rather ductile mode of tension cracking failure occurred on the top of the slab along the column face due to considerable slab folding. Specimens S3 and S4 achieved higher shear stresses than those from Eq. (10), and Specimen S2 almost reached the concrete stress capacity of $(3.5\sqrt{f'_c} + 0.3f_{pc}$. It is noted that actual shear stress capacity appears to be much larger than the maximum monitored v_u, as all specimens except Specimen S4 failed in a ductile manner without, or prior to, punching. If the specimens (for example, Specimens S1 and S2) would be designed with larger flexural capacity (for example, by providing additional bonded steel), shear failure would occur at a much higher v_u (this has been confirmed from an additional analysis); however, such brittle design is not feasible in practice.

Although it appears that the PT specimens had a concrete shear capacity greater than Eq. (10), additional studies on other PT edge connections would be needed to develop recommendations on the punching shear stress capacity of a PT edge connection or to relieve the limitation of $\sqrt{f_c'}$ and/or f_{pc} for PT connections.

Assessment of ACI 318 punching shear provisions of PT edge connections

Table 4 summarizes the test results of direct shear and unbalanced moment at peaks of applied loads, as well as the values of v_u calculated using these experimentally measured values and Eq. (8) and (9), and the values of v_c based on Eq. (10) and ACI 318-08 code provisions. When comparisons are made between the larger of the two values in Columns 10 and 11 of Table 4 and the specified capacity in Column 12 (or Column 13 based on Eq. (10)) of Table 4, it is apparent that the ACI 318 code provisions are overly conservative. Again, note that under applied direct shear and unbalanced moment, the specimens did not undergo punching prior to flexural failure. Furthermore, the back of the critical section (that is, slab edge) was observed to be minimally damaged, as opposed to the values indicated in Table 4 (refer to Column 10 versus Column 11). If the γ_v factor is reduced to one-half of its specified value, the values would make more sense. This exercise verifies the findings obtained from applying nonlinear finite element modeling. It is worth mentioning that in this section, the numerical results of direct shear and unbalanced moment were not used for the assessment.

SUMMARY AND CONCLUSIONS

Realistic modeling of unbonded PT slab-column connections is particularly challenging due to its complex 3-D stress states and nonconventional interaction between unbonded tendons and concrete. In this study, a very sophisticated nonlinear finite element model has been developed to simulate unbonded PT connection behavior. Based on the modeling and calibration studies, the following conclusions were drawn:

1. The accuracy of the unbonded tendon modeling approach has been demonstrated through the direct comparison of overall behavior and damage patterns, moment-drift relations, and unbonded tendon stress increases. The developed nonlinear finite element model performed considerably well for all PT slab-column connections with two different tendon layouts (banded-distributed and distributed-banded) and three different moment-to-shear ratios.

2. The fraction γ_v of the unbalanced moment being transferred by eccentric shear was estimated to be approximately half of the ACI specified value at peak or punching for the edge PT slab-column connections. This indicates that there were moderate interactions between moment and shear and, thus, a decrease in γ_v by 50% (or increase in γ_f by 50%) may be permitted for an edge PT slab-column connection. Additional calibration work, however—perhaps using PT slabs tested by other investigators—would be needed for a thorough investigation on the γ_v factors of PT slab-column connections.

3. The assessment of the γ_v factors indicates that the eccentric shear stress model is valid for PT edge slab-column connections and that there is a certain degree of interaction between moment and shear at the PT edge connection.

4. The punching shear capacity of edge PT slab-column connections appears to be benefitted by the prestress due to PT, as opposed to the ACI 318 code requirements and commentary (Sections 11.11.2.2 and R11.11.2.2). This is the case for both banded-distributed and distributed-banded tendon arrangements; however, to apply Eq. (10) for an edge PT connection, additional studies on other PT connections would be needed. Furthermore, the limitation of $\sqrt{f_c'}$ and/or f_{pc} for PT connections could be relieved.

ACKNOWLEDGMENTS

The work presented in this paper was funded by the University of Oklahoma, Norman, OK. The authors would like to acknowledge PTI Building Design Committee members R. Ahmed, J. Ales, B. Allred, A. Baxi, M. Cuadra, C. Hayek, D. Kline, C. Kopczynski, and M. Vejvoda for their active discussion concerning the design of post-tensioned buildings during committee meetings and conference calls. The views expressed are those of the authors, and do not necessarily represent those of the sponsor or discussers.

REFERENCES

Abaqus, 2003, "User's Manual, Volumes I to III," Hibbitt, Karlson & Sorenson, Inc., 2003, Pawtucket, RI.

ACI Committee 318, 2008, "Building Code Requirements for Structural Concrete (ACI 318-08) and Commentary," American Concrete Institute, Farmington Hills, MI, 2008, 473 pp.

Carreira, D. J., and Chu, K. H., 1985, "Stress-Strain Relationship for Plain Concrete in Compression," ACI JOURNAL, *Proceedings* V. 83, No. 6, Nov.-Dec. 1985, pp. 797-804.

Devalapura, R. K., and Tadros, M. K., 1992, "Critical Assessment of ACI 318 Eq. (18-3) for Prestressing Steel Stress at Ultimate Flexure," *ACI Structural Journal*, V. 89, No. 5, Sept.-Oct. 1992, pp. 538-546.

Foutch, D. A.; Gamble, W. L.; and Sunidja, H., 1990, "Tests of Post-Tensioned Concrete Slab-Edge Column Connections," *ACI Structural Journal*, V. 87, No. 2, Mar.-Apr. 1990, pp. 167-179.

Hillerborg, A.; Modeer, M.; and Petersson, P. E., 1976, "Analysis of Crack Formation and Crack Growth in Concrete by Means of Fracture Mechanics and Finite Elements," *Cement and Concrete Research*, V. 6, 1976, pp. 773–782.

Huang, Y.; Kang, T. H.-K.; Ramseyer, C.; and Rha, C., 2010, "Background to Multi-Scale Modeling of Unbonded Post-Tensioned Concrete Structures," *International Journal of Theoretical and Applied Multiscale Mechanics*, Inderscience.

Kang, T. H.-K., and Wallace, J. W., 2008, "'Stresses in Unbonded Tendons of Post-Tensioned Flat Plate Systems under Dynamic Excitation," *PTI JOURNAL*, V. 6, No. 1, Feb., pp. 31-44.

Kang, T. H.-K.; Wallace, J. W.; and Elwood, K. J., 2009, "Nonlinear Modeling of Flat-Plate Systems," *Journal of Structural Engineering*, ASCE, V. 135, No. 2, Feb., pp. 147-158.

Nilson, A. H.; Darwin, D.; and Dolan, C. W., 2009, "Design of Concrete Structures," fourteenth edition, McGraw Hill, New York, 816 pp.

Park, H.-G., and Choi, K.-K., 2006, "Improved Strength Model for Interior Flat Plate-Column Connections Subject to Unbalanced Moment," *Journal of Structural Engineering*, ASCE, V. 132, No. 5, May, pp. 694-704.

Park, H.-G., and Choi, K.-K., 2007, "Strength of Exterior Slab-Column Connections Subjected to Unbalanced Moments," *Engineering Structures*, V. 29, Elsevier, June, pp. 1096-1114.

Park, R., and Gamble, W. L., 2000, *Reinforced Concrete Slabs*, John Wiley & Sons, Inc., second edition, New York, pp. 736.

Smith, S. W., and Burns, N. H., 1974, "Post-Tensioned Flat Plate to Column Connection Behavior," *PCI Journal*, V. 19, No. 3, May-June, pp. 74-91.

Tian, Y.; Jirsa, J. O.; Bayrak, O.; Widianto; and Arqudo, J. F., 2008, "Behavior of Slab-Column Connections of Existing Flat-Plate Structures," *ACI Structural Journal*, V. 105, No. 5, Sept.-Oct., pp. 561-569.

Trongtham, N., and Hawkins, N. M., 1977, "Moment Transfer to Columns in Unbonded Post-Tensioned Prestressed Concrete Slabs," *Report* SM77-3, Department of Civil Engineering, University of Washington, Seattle, WA, 1977, 186 pp.

PTI Fellow ***Thomas H.-K. Kang*** *is an Assistant Professor of civil engineering at Seoul National University, Seoul, Korea. Before that, he was an Assistant Professor at the University of Oklahoma, Norman, OK. He is a licensed professional engineer in California. He received his PhD from the University of California (UCLA), Los Angeles, CA, and his BS from Seoul National University. He is a member of PTI Committee DC-20, Building Design. His research interests include design and rehabilitation of post-tensioned buildings and systems.*

Yu Huang *received his PhD from the University of Oklahoma and his BS from ChongQing JiaoTong University, China. His research interests include finite element analyses of reinforced and post-tensioned concrete systems.*